9-4-2018

Unconventional Anomalous Hall Effect from Antiferromagnetic Domain Walls of $Nd_2Ir_2O_7$ Thin Films

Woo Jin Kim
Institute for Basic Science, South Korea

John H. Gruenewald
University of Kentucky, john.gruenewald@uky.edu

Taekoo Oh
Institute for Basic Science, South Korea

Sangmo Cheon
Hanyang University, South Korea

Bongju Kim
Institute for Basic Science, South Korea

See next page for additional authors

Authors
Woo Jin Kim, John H. Gruenewald, Taekoo Oh, Sangmo Cheon, Bongju Kim, Oleksandr B. Korneta, Hwanbeom Cho, Daesu Lee, Yoonkoo Kim, Miyoung Kim, Je-Geun Park, Bohm-Jung Yang, and Ambrose Seo

Unconventional Anomalous Hall Effect from Antiferromagnetic Domain Walls of $Nd_2Ir_2O_7$ Thin Films

Notes/Citation Information
Published in *Physical Review B*, v. 98, issue 12, 125103, p. 1-9.

Digital Object Identifier (DOI)
https://doi.org/10.1103/PhysRevB.98.125103

Unconventional anomalous Hall effect from antiferromagnetic domain walls of $Nd_2Ir_2O_7$ thin films

Woo Jin Kim,[1,2] John H. Gruenewald,[3] Taekoo Oh,[1,2,4] Sangmo Cheon,[5] Bongju Kim,[1,2] Oleksandr B. Korneta,[1,2] Hwanbeom Cho,[1,2] Daesu Lee,[1,2] Yoonkoo Kim,[6] Miyoung Kim,[6] Je-Geun Park,[1,2] Bohm-Jung Yang,[1,2,4] Ambrose Seo,[3] and Tae Won Noh[1,2,*]

[1]*Center for Correlated Electron Systems, Institute for Basic Science, Seoul 08826, Republic of Korea*
[2]*Department of Physics and Astronomy, Seoul National University, Seoul 08826, Republic of Korea*
[3]*Department of Physics and Astronomy, University of Kentucky, Lexington, Kentucky 40506, USA*
[4]*Center for Theoretical Physics, Seoul National University, Seoul 08826, Republic of Korea*
[5]*Department of Physics, Hanyang University, Seoul 04763, Republic of Korea*
[6]*Department of Materials Science and Engineering and Research Institute of Advanced Materials, Seoul National University, Seoul 08826, Republic of Korea*

(Received 1 December 2017; revised manuscript received 12 April 2018; published 4 September 2018)

Ferroic domain walls (DWs) create different symmetries and ordered states compared with those in single-domain bulk materials. In particular, the DWs of an antiferromagnet with noncoplanar spin structure have a distinct symmetry that cannot be realized in those of their ferromagnet counterparts. In this paper, we show that an unconventional anomalous Hall effect (AHE) can arise from the DWs of a noncoplanar antiferromagnet, $Nd_2Ir_2O_7$. Bulk $Nd_2Ir_2O_7$ has a cubic symmetry; thus, its Hall signal should be zero without an applied magnetic field. The DWs generated in this material break the twofold rotational symmetry, which allows for finite anomalous Hall conductivity. A strong f-d exchange interaction between the Nd and Ir magnetic moments significantly influences antiferromagnetic (AFM) domain switching. Our epitaxial $Nd_2Ir_2O_7$ thin film showed a large enhancement of the AHE signal when the AFM domains switched, indicating that the AHE is mainly due to DWs. Our paper highlights the symmetry-broken interface of AFM materials as a means of exploring topological effects and their relevant applications.

DOI: 10.1103/PhysRevB.98.125103

I. INTRODUCTION

Both symmetry and the ferroic order inevitably become modified in a ferroic domain wall (DW), triggering new functions and topological properties [1–6]. The discovery of conductive DWs in ferroelectric thin films opened a broad field of research dedicated to understanding the underlying mechanisms, and the fabrication of practical DW-based devices [1–4]. The DWs of certain ferromagnets exhibit topological Hall effects attributable to magnetic skyrmions [5,6]. However, similar topological properties have yet to be observed in the DWs of antiferromagnets. Although there exists a theoretical prediction that a finite anomalous Hall effect (AHE) can arise among antiferromagnetic (AFM) DWs with nonvanishing Berry curvatures [7], few experimental studies have investigated this intriguing possibility.

Since Wan *et al.* theoretically proposed the existence of a Weyl fermionic state in AFM-ordered $Y_2Ir_2O_7$ [8], the rare-earth pyrochlore iridates have attracted great interest [9]. Particularly, $Nd_2Ir_2O_7$ has been widely studied, due to its proximity to the metal-insulator transition (MIT) [10,11] and large DW conductance [12]. To discuss the AFM spin structure in detail, consider that $Nd_2Ir_2O_7$ is composed of two types of tetrahedra, Ir and Nd sublattices, as shown in Fig. 1(a). As shown by the red arrows, all four of the Ir spins at the vertices of a tetrahedron point inward. At the nearest-neighbor Ir tetrahedra (not shown), all of the Ir spins should point outward. This results in all-in–all-out (AIAO) ordering of Ir spins, which we refer to as Ir:AIAO. At the same time, the spins in the Nd sublattice have similar magnetic ordering (all-out–all-in), Nd:AOAI, as shown in Fig. 1(a). These intriguing magnetic orderings and coupling between two different sublattices play important roles in the physical properties of these materials [8–14].

Under an external magnetic field, H, we can switch between AIAO and AOAI domains of Ir spin. It is important to understand how DWs can be formed during the switching process in a $Nd_2Ir_2O_7$ sample. Note that the Nd ion has a larger magnetic moment; thus, the corresponding Zeeman field is larger. When H increases along the [111] direction, Nd spins become canted and then suddenly flip to form the three-in–one-out (3I1O) configuration [15]. At a higher H, Nd spins can induce a flip of the Ir sublattice spin into the AOAI configuration via the f-d exchange interaction [see Fig. 1(b)]. During this spin switching process, two kinds of domains may coexist, resulting in the presence of DWs [see Fig. 1(c)].

Here, we present a $Nd_2Ir_2O_7$ epitaxial thin film as an ideal system for realizing the intriguing topological responses that originate from the DWs of an AFM material. The electronic structure of $Nd_2Ir_2O_7$ has been assumed to be close to that of a Weyl semimetal [8,16]. This similarity to a semimetallic ground state results in a very large DW conductance [12,15]. Within a single AIAO or AOAI domain, AHE is forbidden

*twnoh@snu.ac.kr

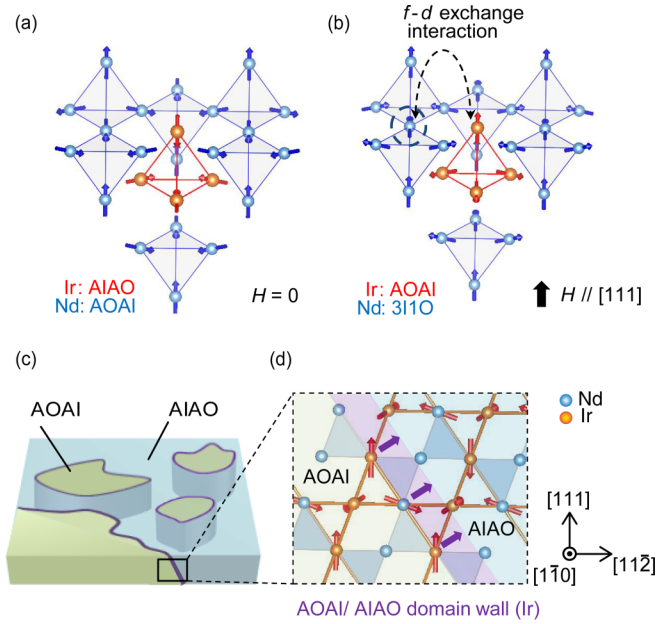

FIG. 1. Schematic diagrams of the magnetic domain structure of $Nd_2Ir_2O_7$. (a) The magnetic structure of Nd $4f$ moments (blue arrows) and Ir $5d$ moments (red arrows) at $H = 0$ and temperatures below T_N^{Nd}. The Ir and Nd sublattices have all-in–all-out (AIAO) and all-out–all-in (AOAI) ordering, respectively. (b) The magnetic structure in sufficiently strong H. The Nd $4f$ and Ir $5d$ moments are coupled with the f-d exchange interaction. (c) Schematic diagram of the DWs between Ir-AIAO and Ir-AOAI. The purple-colored line indicates the possible DW structure with finite magnetization. (d) Schematic diagram of the dotted square region in (c), enlarged for detail. The purple arrows indicate the net magnetization of Ir moments at a DW.

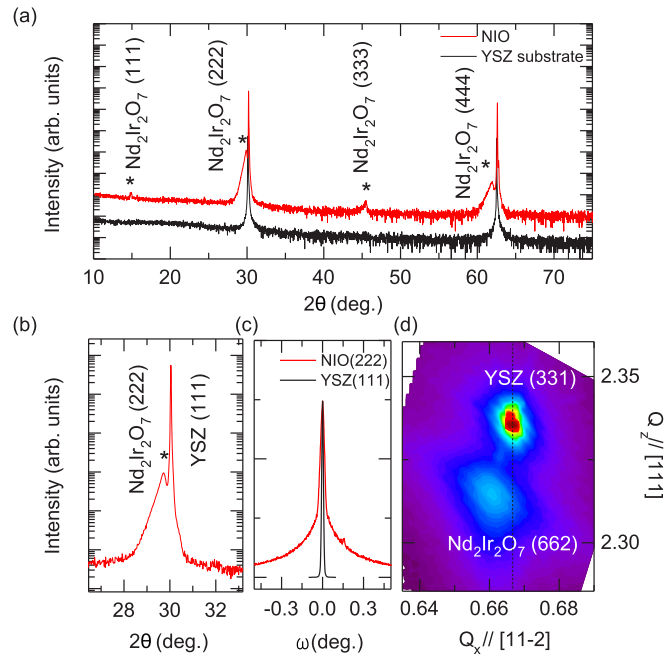

FIG. 2. (a) X-ray-diffraction pattern of an 80-nm-thick $Nd_2Ir_2O_7$ thin film grown on a YSZ (111) substrate (red bold line) and the diffraction pattern of the bare YSZ substrate (black bold line). (b) $Nd_2Ir_2O_7$ (222) diffraction pattern. (c) Rocking curve of $Nd_2Ir_2O_7$/YSZ (111) thin film. (d) Reciprocal space map of $Nd_2Ir_2O_7$ (662).

by cubic crystalline symmetry [17,18]. However, in the presence of a DW, we show that twofold rotation symmetries are explicitly broken, resulting in uncompensated magnetic moments (see Sec. IV C). This leads to a finite anomalous Hall conductivity in the plane parallel to the highly conducting DW. Thus, it is informative to explore DW-induced unconventional magnetotransport in low-dimensional $Nd_2Ir_2O_7$ thin films, in which the contribution of the DW can be maximized [19].

II. EXPERIMENTS

A. Deposition of $Nd_2Ir_2O_7$ thin films

We prepare $Nd_2Ir_2O_7$ (111) thin films on commercial Y-stabilized ZrO_2 (YSZ) (111) single-crystal substrates via pulsed laser deposition followed by a postannealing procedure. We irradiate a single-phase $Nd_2Ir_2O_7$ polycrystalline target with a KrF excimer laser ($\lambda = 248$ nm); the laser fluence and frequency were 4.5 J/cm^2 and 3 Hz, respectively. We maintain the distance between the target and the substrate at 50 mm. It is well known that pyrochlore iridate thin films are extremely difficult to deposit because of the volatility of iridium [20–22]. To form the pyrochlore phase thermodynamically, it is required to use a high oxygen pressure and a high temperature during thin film deposition [23]. When we deposit pyrochlore iridate thin films under such conditions, the gas phase of IrO_3 is likely to form and evaporate, posing extreme difficulties for *in situ* growth. We initially deposit stoichiometric amorphous $Nd_2Ir_2O_7$ thin films at 600 °C. Following deposition, we postanneal the thin films in air in an electrical box furnace at 1000 °C for 1 h [24].

Figure 2(a) shows x-ray-diffraction (XRD) θ-2θ scans of our $Nd_2Ir_2O_7$ thin film and the YSZ substrate. The figure shows only peaks from plane parallel to $Nd_2Ir_2O_7$ (111) in addition to substrate peaks, indicating that the thin film is a single phase. Figure 2(b) shows the detailed XRD pattern near the $Nd_2Ir_2O_7$ (222) peak. Figure 2(c) shows that the full width at half maximum of the rocking curve is ∼0.05°, indicating that the sample is highly crystalline. We utilize x-ray reciprocal space mapping (X-RSM) to measure the in-plane lattice constants of the thin film and substrate. Figure 2(d) shows X-RSM data around the (662) and (331) Bragg reflections of the $Nd_2Ir_2O_7$ thin film and YSZ substrate, respectively. The (662) Bragg peak of the $Nd_2Ir_2O_7$ thin film has smaller Q_x and Q_z values than those of the YSZ (331) Bragg peak. From the experimental Q_x and Q_z values, the lattice constants of our thin film are estimated to be $a = b = 10.380$ Å, close to those of bulk polycrystalline $Nd_2Ir_2O_7$ ($a = b = c = 10.375$ Å). This indicates that our thin films have high structural quality close to the bulk counterparts.

B. Scanning transmission electron microscopy measurements

We utilize scanning transmission electron microscopy (STEM) to explore the microstructure of our $Nd_2Ir_2O_7$ thin films. Figure 3(a) shows a STEM image of an $Nd_2Ir_2O_7$ thin

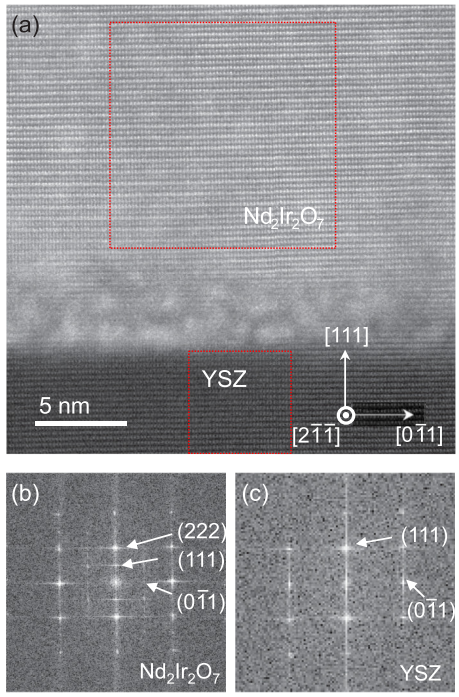

FIG. 3. (a) STEM image of an $Nd_2Ir_2O_7$ thin film deposited on YSZ (111) from the viewpoint of the $[2\bar{1}\bar{1}]$ axis. The $Nd_2Ir_2O_7$ thin film exhibits an ordered pyrochlore structure and an epitaxial relationship with the YSZ substrate. (b) The fast Fourier transform of the pyrochlore $Nd_2Ir_2O_7$ thin film (upper red dashed square) and (c) that of the YSZ substrate (lower red dashed square).

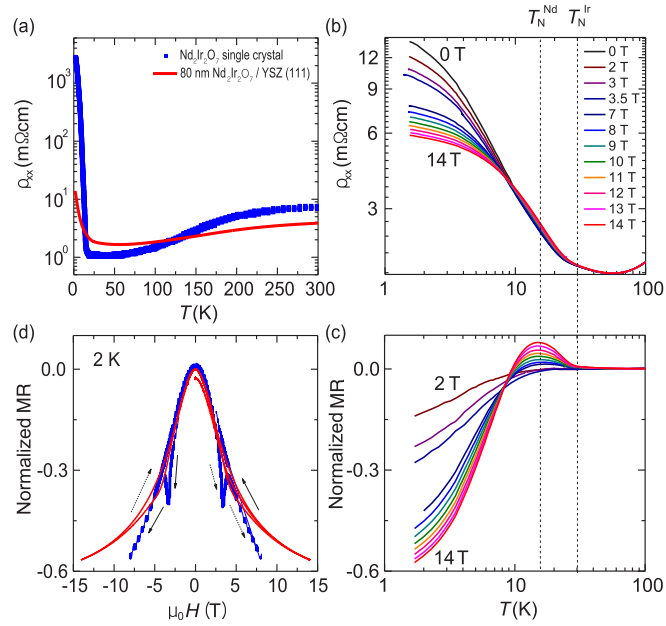

FIG. 4. (a) Temperature dependence of the longitudinal resistivity ρ_{xx} of the 80-nm-thick film (red bold line) and its counterpart of single crystal from Ref. [15] (blue square). (b) Temperature-dependent magnetoresistance (MR) of $Nd_2Ir_2O_7$ for various $H \parallel [111]$ from 0 to 14 T. The T_N^{Nd} (∼15 K) and T_N^{Ir} (∼30 K) indicate the Néel temperature of the Nd and Ir moments, respectively. (c) Corresponding normalized MR values vs temperature. When H is sufficiently large, the gradient of the MR changes from positive to negative at T_N^{Nd}. (d) Normalized MR values with $H \parallel [111]$ at 2 K of the 80-nm-thick film (red bold line) and a single crystal from Ref. [15] (blue square).

film on a YSZ (111) substrate with the zone axis parallel to $[2\bar{1}\bar{1}]$. A blurry region is evident near the interface between thin film and substrate, which may be attributable to defects and/or electron-beam damage during STEM measurements. To determine structural relationships, we perform fast Fourier transforms (FFTs) of real-space images of the $Nd_2Ir_2O_7$ thin film and the YSZ substrate region [see Figs. 3(b) and 3(c)]. Although our thin films are deposited by postannealing the amorphous phase, an epitaxial relationship is evident between $Nd_2Ir_2O_7$ and the YSZ substrate: $Nd_2Ir_2O_7[111] \parallel$ YSZ[111] and $Nd_2Ir_2O_7$ $[0\bar{1}1] \parallel$ YSZ $[0\bar{1}1]$.

C. Resistivity and magnetotransport measurements

We measure dc magnetotransport properties below ∼14 T using the standard four-probe method and a commercial cryostat system (Oxford Instruments). For higher H fields up to 30 T, we utilize the resistive magnet at the National High Magnetic Field Laboratory. During these magnetotransport measurements, we apply current along the $[1\bar{1}0]$ direction and H along the [111] direction (i.e., perpendicular to the current direction). In Fig. 4(a), our 80-nm-thick $Nd_2Ir_2O_7$ thin film exhibits a MIT around $T_N^{Ir} \sim 30$ K, close to the bulk value. On the other hand, the associated resistivity ratio, $\rho(2\,\mathrm{K})/\rho(300\,\mathrm{K})$, is much broader than that of the "best" single-crystalline sample [15]. The resistivity ratio, $\rho(2\,\mathrm{K})/\rho(300\,\mathrm{K})$, is ∼10, which is much smaller than the compared value (∼1000) of the single crystal. However, it should be noted that the reported resistivity ratio values in literature vary in a wide range of 10–1000 even for single crystals [25]. Therefore, our $Nd_2Ir_2O_7$ thin films has crystal quality at least comparable to some single crystals [25].

To measure magnetoresistance (MR) behavior, we zero-field cooled the $Nd_2Ir_2O_7$ thin film to 2 K and measured resistivity under a constant H field while warming to 300 K. In Fig. 4(b), the resistance changes under a H field are large but become smaller as T increases, vanishing around T_N^{Ir}. Figure 4(c) shows T-dependent normalized MR curves at various H values. The MR peaks at ∼15 K, which corresponds to the Néel ordering temperature of the Nd moment (T_N^{Nd}) [26].

III. ANTIFERROMAGNETIC DOMAIN SWITCHING

A. Magnetoresistance hysteresis

Figure 4(d) shows a H-dependent normalized MR curve at 2 K, where the comparison with the single crystal data in Ref. [15] can be made. Note that it exhibits an intriguing hysteretic behavior with very broad MR dips around ±3 T. This feature is somewhat broad, since it may come from many inherent defects inside the thin film and pining of DWs to such defects. However, this hysteretic behavior is essentially similar to that of the single crystal, which is marked by the blue square line. The MR dips occurs around ±3 T, nearly at the magnetic coercive field H_C of the single crystal [15]. In addition, the hysteresis direction is the same as that in

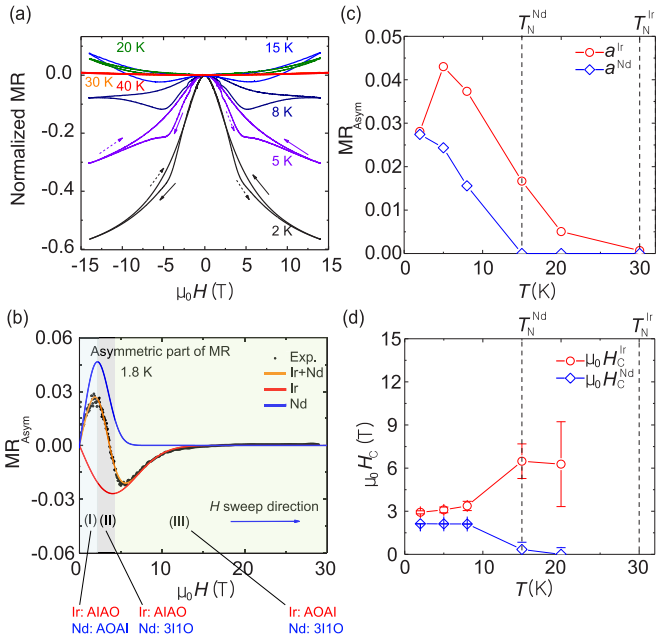

FIG. 5. (a) Normalized MR at various temperatures with $H \parallel [111]$. (b) Asymmetric component of the sweep-up MR at 1.8 K (positive H). The colored region with roman numerals corresponds to the represented spin structures. The red (blue) and orange solid lines indicate the hysteretic part of Ir (Nd) domain switching from Eq. (2) and its total contribution to both Nd and Ir, respectively. (c) Quantified fit parameters a extracted from Eq. (2), where red empty circles (blue empty diamonds) indicate the contribution of hysteretic behavior from Ir (Nd) domain switching. (d) Red empty circles and blue empty diamonds are the coercive fields of the Ir domain and Nd spins, respectively, from MR. At 30 K, the asymmetric MR becomes too small to obtain reliable values of the coercive field.

the single-crystal data, suggesting that the magnetic hysteresis might come from DW switching.

Such hysteretic behavior is also evident at other temperatures below T_N^{Ir}. Figure 5(a) shows normalized MR curves with H along the [111] direction at various temperatures. The MR is positive at higher T but becomes negative around $T_N^{Nd} \sim 15$ K [26], consistent with Fig. 4(c). Note that the dip structures in the MR hysteresis curve can be easily observed between 5 and 15 K. These structures occur at the magnetic fields that are close to the reported H_C values of single crystals [15]. In an earlier work, the hysteretic MR behavior is already attributed to AFM domain switching [27]. Likewise, our MR data can be explained in terms of switching between the AIAO and AOAI domains.

B. Asymmetric analysis on hysteretic magnetoresistance curves

In the hysteresis curve of a ferroic material, it is well known that the asymmetric MR part contains important information on magnetic domain switching [24,28]. We extract the asymmetric part of the normalized MR curves using

$$\mathrm{MR}_{\mathrm{Asym}}(H) = \frac{\rho_{xx}(H) - \rho_{xx}(-H)}{2\rho_{xx}(0)}. \quad (1)$$

Figure 5(b) shows the $\mathrm{MR}_{\mathrm{Asym}}(H)$ curve at 1.8 K with increasing H field from -30 to 30 T [only the positive side is plotted, given that $\mathrm{MR}_{\mathrm{Asym}}(-H) = -\mathrm{MR}_{\mathrm{Asym}}(H)$]. Note the interesting structures in the $\mathrm{MR}_{\mathrm{Asym}}(H)$ curve: a peak at low H and a dip at high H. Additionally, the curve displays a sign change in $\mathrm{MR}_{\mathrm{Asym}}(H)$ around 3.0 T. To our knowledge these $\mathrm{MR}_{\mathrm{Asym}}(H)$ behaviors have not been observed in other magnetic ferroic materials.

Using detailed analysis of the MR curves, we can obtain insight into spin-ordering and DW dynamics. It is well established in most ferroic materials that domain switching usually occurs at H_C. When switching becomes broadened due to pinning of DWs to defects and/or surfaces, the H_C distribution in DW switching dynamics can be fitted with a Gaussian function [29,30]. To account for the asymmetry, we fit our $\mathrm{MR}_{\mathrm{Asym}}(H)$ data with an asymmetric Gaussian function:

$$\mathrm{MR}_{\mathrm{Asym,\ FIT}}(H) = a\left(e^{-b(H-H_c)^2} - e^{-b(H+H_c)^2}\right), \quad (2)$$

where a and b are the magnitude and width of the hysteretic behavior, respectively.

We find that the associated sign change in $\mathrm{MR}_{\mathrm{Asym}}(H)$ in Fig. 5(b) cannot be fit with a single asymmetric Gaussian function in Eq. (2). This indicates that the hysteresis cannot be explained in terms of magnetic switching in one kind of sublattice, i.e., either Ir or Nd spins. On the other hand, when we introduce two magnetic switching functions (namely, the two asymmetric Gaussian functions), we are able to fit the experimental $\mathrm{MR}_{\mathrm{Asym}}(H)$ curves quite well. In Fig. 5(b), we plot the red (blue) line for higher-field (lower-field) magnetic switching. These indicate that both Ir and Nd spins are involved with magnetotransport properties of our $Nd_2Ir_2O_7$ thin films.

Considering the T_N of each ion, we find that the switching at the higher (lower) H_c value is the result of the Ir (Nd) sublattice. Figure 5(c) shows the temperature dependence of each respective ion's fit coefficient (a) calculated from the symmetry analysis of $\mathrm{MR}_{\mathrm{Asym}}(H)$ curves. As the temperature is decreased, the a value of the red line first appears around 30 K ($\sim T_N^{Ir}$). This coincides with Ir spin ordering; thus, we can assign the red line to a^{Ir}. Likewise, the blue line begins to emerge around T_N^{Nd} and monotonically increases, thus corresponding to a^{Nd}. Note that the values of a^{Ir} are larger than those of a^{Nd}. As the conduction in $Nd_2Ir_2O_7$ occurs in the Ir-O network [9], it is reasonable to expect the Ir spins to dominate the change in MR. Therefore, the red and blue lines in Fig. 5(b) should correspond to the switching of spins of Ir and Nd sublattices, respectively.

C. Domain switching caused by the f-d exchange interaction

Figure 5(b) shows that the switching of Nd spins occurrs at lower H than that of Ir spins. Based on the relative values of the switching H field, we can summarize the domain switching sequence as follows: (1) at small H, the Ir-AIAO domains dominate, along with Nd-AOAI spin structures; (2) as H increases, Nd spins flip first to form Nd-3I1O while the Ir sublattice remains in the Ir-AIAO configuration; and (3) finally, at higher H, the Nd-3I1O spin structure flips the Ir spins, resulting in the formation of Ir-AOAI domains. This switching sequence is consistent with that described in Fig. 1.

The MR data also indicate that Ir and Nd spins are strongly coupled, presumably due to the f-d exchange interaction.

From the T-dependent analysis of $\mathrm{MR}_{\mathrm{Asym}}(H)$, we are able to determine the coercive fields required to switch the spins of each Ir and Nd sublattice. The fitted values for $\mu_0 H_C^{\mathrm{Nd}}$ are shown as blue open diamonds in Fig. 5(d). Nd spin switching does not occur for $T > T_{\mathrm{N}}^{\mathrm{Nd}}$. Below $T_{\mathrm{N}}^{\mathrm{Nd}}$, $\mu_0 H_C^{\mathrm{Nd}}$ increases and remains nearly constant around 2 T. The fitted values for $\mu_0 H_C^{\mathrm{Ir}}$ are shown as red open circles. Ir-AIAO to AOAI domain switching begins below $T_{\mathrm{N}}^{\mathrm{Ir}}$, i.e., $H_C^{\mathrm{Ir}} \sim 7$ T around 20 K. The MR signal becomes small close to $T_{\mathrm{N}}^{\mathrm{Ir}}$, making it difficult to estimate a value for H_C^{Ir}. As the temperature decreases, $\mu_0 H_C^{\mathrm{Ir}}$ decreases abruptly below $T_{\mathrm{N}}^{\mathrm{Nd}}$ and then remains nearly constant around 3 T. Note that the extraordinary decrease of H_C^{Ir} around $T_{\mathrm{N}}^{\mathrm{Nd}}$ cannot occur in magnetic systems with a single magnetic sublattice. This surprising behavior emphasizes the important role of the f-d exchange interaction in Ir domain switching of the pyrochlore iridate thin film.

IV. ANOMALOUS HALL EFFECTS CAUSED BY ANTIFERROMAGNETIC DOMAIN WALLS

A. AHEs observed in $Nd_2Ir_2O_7$ thin films

We measure the transverse magnetoresistance, i.e., Hall resistivity ρ_{xy}, of our $Nd_2Ir_2O_7$ thin films with H along the [111] direction. Figure 6(a) shows that the ρ_{xy} curves have a very large and unconventional Hall resistivity behavior. As the temperature decreases below 30 K, hysteretic behavior with a "humplike" peak is observed, which cannot be explained by the conventional ordinary Hall effect. This hysteretic behavior with humplike peak intensity becomes more pronounced as the temperature decreases below $T_{\mathrm{N}}^{\mathrm{Nd}}$. Similar humplike behavior has been observed in ferromagnetic DWs and has been attributed to the presence of a real-space topological Hall effect related to magnetic skyrmions [5,6].

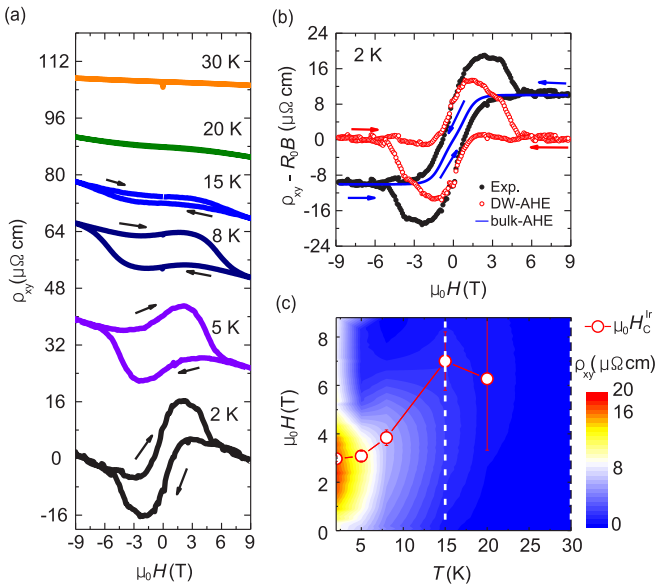

FIG. 6. (a) H dependence of the Hall resistivity taken with $H \parallel$ [111] at various temperatures. The arrows indicate the H sweep directions. (b) Black empty circles indicate the Hall resistivity at 2 K. The ordinary Hall term is subtracted by linear fitting in the higher H region. The blue solid lines indicate the contribution of the bulk AHE. The red circles indicate the DW AHE. (c) Color map of anomalous Hall resistivity (ordinary Hall term is subtracted) in the T-H plane. The red empty circles represent the coercive field H_c^{Ir} of Ir domain switching, which are obtained from MR measurements.

To obtain further insight into the AHE, we subtracted the H-linear ordinary Hall effect term from the 2-K ρ_{xy} data and plotted the data as black solid circles in Fig. 6(b). In the figure, the AHE term peaks around 2–3 T. The corresponding H value is close to the $\mu_0 H_C^{\mathrm{Ir}}$ values, obtained from the earlier MR data analysis. It indicates that a DW could play a significant role in the observed AHE. In addition, the experimental AHE reaches a nearly constant value above 5 T, suggesting that bulk effects may also be involved. These results suggest that the AHE may have originated from both bulk and DW contributions, hereafter referred to as bulk AHE and DW AHE, respectively.

B. Bulk AHE of antiferromagnetic material: Scalar spin chirality

For AFM bulk materials, AHEs have been observed and explained in terms of the scalar spin chirality. This term can be defined as $\vec{S}_i \cdot (\vec{S}_j \times \vec{S}_k)$ with three local spins $\vec{S}_i$, $\vec{S}_j$, and $\vec{S}_k$ [31]; the scalar product corresponds to the solid angle Ω subtended by the three spins. The noncoplanar spin configuration is closely linked to the Berry curvature and can generate a fictitious magnetic flux proportional to the scalar spin chirality. As a result, an AHE can occur [32–39]. Without a magnetic field, the total magnetization and scalar spin chirality remain zero inside a single $Nd_2Ir_2O_7$ magnetic domain. However, applying a strong magnetic field changes the order of the Nd moments to 3I1O [see Fig. 1(b)] and Ir moments to a canted AIAO. Then, both magnetization and scalar spin chirality become finite, and the canted antiferromagnet exhibits finite bulk AHE.

Let us estimate the ρ_{xy} values attributable to the bulk AHE for $Nd_2Ir_2O_7$. Note that the AIAO (AOAI) order of the Ir moments is canted by the 1I3O (3I1O) order of the Nd moments via the f-d exchange interaction. As a result, the scalar spin chirality is produced in the Ir spin system and generates a fictitious magnetic field parallel to its magnetization direction [40]. Moreover, it is well known that the Nd moments ($\sim$2.4 μ_{B}/Nd) are much larger than the Ir moments ($\sim$0.2 μ_{B}/Ir) [15]. As the magnetic moment of Ir is an order of magnitude smaller than that of Nd, the Ir sublattice makes a much smaller contribution to the magnetization. Given that both the scalar spin chirality term of Ir spins and total magnetization are dominated by Nd moments, we will focus on the spin configuration in Nd tetrahedrons, changing from AIAO to 3I1O. We can quantify the proportions of Nd unit cells in the 3I1O order by calculating the expectation value of magnetization per unit cell. Then we can infer a bulk Hall resistivity curve, which is proportional to the number of Nd unit cells in the 3I1O order.

To quantitatively estimate the H-dependent net magnetization of the Nd sublattice, we consider the Hamiltonian below, which describes a single Nd unit cell in a magnetic field along

the direction of the [111] plane:

$$H = -J \sum_{\langle ij \rangle} \vec{S_i} \cdot \vec{S_j} - \mu \vec{B} \cdot \sum_i \vec{S_i} - K \Phi B_x B_y B_z, \quad (3)$$

where J is the interaction strength, μ is the Bohr magneton, and $\vec{B}$ is magnetic field. K is a coefficient and Φ is the AIAO order parameter expressed as

$$\Phi = \frac{1}{4\sqrt{3}}(S_{1x} + S_{1y} + S_{1z} + S_{2x} - S_{2y} - S_{2z} - S_{3x} + S_{3y} - S_{3z} - S_{4x} - S_{4y} + S_{4z}). \quad (4)$$

Here, we treat the Nd spin as an Ising variable. The spin vector at each site in a unit cell is defined as $\vec{S_1} = \frac{\sigma_1}{\sqrt{3}}(1,1,1)$, $\vec{S_2} = \frac{\sigma_2}{\sqrt{3}}(1,-1,-1)$, $\vec{S_3} = \frac{\sigma_3}{\sqrt{3}}(-1,1,-1)$, and $\vec{S_4} = \frac{\sigma_4}{\sqrt{3}}(-1,-1,1)$, where $\sigma_i = \pm 1$. Then, Eq. (3) can be simplified to

$$H = -J \sum_{\langle ij \rangle} \sigma_i \sigma_j - \mu \vec{B} \cdot \sum_i \vec{S_i} - K \Phi B_x B_y B_z. \quad (5)$$

When $J > 0$, the ground state of the Hamiltonian in a Nd unit cell is AIAO or AOAI ordered without the magnetic field; namely, σ_i is either $+1$ or -1. As such, the expectation value of the magnetization can be calculated using a partition function. For the unit cell, the partition function is

$$Z = \sum_{\sigma_1,\sigma_2,\sigma_3,\sigma_4=\pm 1} \exp(-\beta H), \quad (6)$$

and the expectation value of magnetization along the [111] direction is

$$\langle M \rangle = \frac{1}{Z} \sum_{\sigma_1,\sigma_2,\sigma_3,\sigma_4=\pm 1} \left(\sigma_1 - \frac{1}{3}(\sigma_2 + \sigma_3 + \sigma_4)\right) \exp(-\beta H). \quad (7)$$

We evaluated the bulk AHE of our $Nd_2Ir_2O_7$ thin film by assuming that it should be proportional to the magnetization. Given a sufficient H field, all of the DWs should disappear, such that the DW AHE becomes negligible and the bulk AHE dominates. Using the experimental values of the saturated Hall resistivity value ($\sim 8\,\mu\Omega\,$cm) at $\sim 2\,$T ($\mu_0 H_C^{\mathrm{Nd}}$) in Fig. 6(b), we derived an analytical estimate of the bulk AHE contribution. The bulk-AHE contribution is shown as the blue line in Fig. 6(b). It should be noted that the bulk AHE alone cannot explain the experimental AHE. There should an additional AHE, which cannot be explained by the scalar spin chirality effect.

C. Emergence of the AHE in the presence of an AFM domain wall: Symmetry analysis

We considered the possible emergence of the AHE due to momentum space Berry curvature by performing symmetry analysis. First, we should note that the anomalous Hall conductivity cannot occur in a single domain of AIAO order in cubic pyrochlore iridates [17]. To calculate the intrinsic anomalous Hall conductivity, we integrate the Berry curvature of the occupied bands in momentum space:

$$\sigma_{\alpha\beta} = \frac{e^2}{\hbar} \int_{\mathrm{BZ}} \frac{d^3k}{(2\pi)^3} \sum_n f(\epsilon_n(\vec{k}) - \mu) F_{\alpha\beta}(\vec{k}), \quad (8)$$

where $f(\epsilon_n(\vec{k}) - \mu)$ is the Fermi-Dirac distribution, and $F_{\alpha\beta}$ is the Berry curvature of the $\alpha\beta$ plane. For convenience, we denote each component of the Berry curvature in a vector notation, i.e., $F^x(\vec{k}) = F_{yz}(\vec{k})$, $F^y(\vec{k}) = F_{zx}(\vec{k})$, and $F^z(\vec{k}) = F_{xy}(\vec{k})$. When twofold rotation symmetry around the z axis (C_{2z}) exists, as in the single domain of AIAO (or AOAI) order, $F^x(-k_x,-k_y,k_z) = -F^x(k_x,k_y,k_z)$, $F^y(-k_x,-k_y,k_z) = -F^y(k_x,k_y,k_z)$, and $F^z(-k_x,-k_y,k_z) = F^z(k_x,k_y,k_z)$. Then σ_{yz}, σ_{zx} should be trivial, but σ_{xy} does not have to be trivial through Eq. (8). In a single domain of AIAO order, cubic pyrochlore iridates have C_{2x}, C_{2y}, and C_{2z} symmetry; thus, AHEs cannot occur.

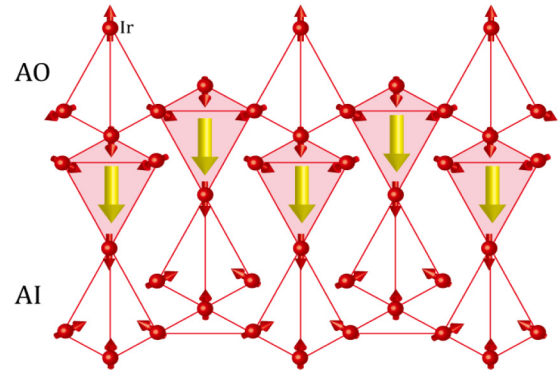

FIG. 7. As an iridium DW in the bulk breaks the twofold rotation symmetry in pyrochlore iridates, causing the anomalous Hall conductivity to be nontrivial. Due to the remaining symmetries with a DW, finite anomalous Hall conductivity can arise on the plane parallel to the DW.

However, in the presence of a DW, an unconventional AHE can be generated from the nonzero Berry curvature. At the DW, twofold rotation symmetries become broken but there exists a threefold rotational symmetry about the axis perpendicular to the DW (see Fig. 7). Considering the threefold rotation axis as [111] and taking the two other perpendicular axes as $[0\bar{1}1]$ and $[\bar{2}11]$, the symmetry properties of the Berry curvature under threefold rotational symmetry are $F^x(k_y,k_z,k_x) = F^y(k_x,k_y,k_z)$, $F^y(k_y,k_z,k_x) = F^z(k_x,k_y,k_z)$, and $F^z(k_y,k_z,k_x) = F^x(k_x,k_y,k_z)$. Using these properties, we establish the properties of the Berry curvature components along [111] as

$$F^{[111]}(\vec{k}) + F^{[111]}(C\vec{k}) + F^{[111]}(C^{-1}\vec{k}) \neq 0, \quad (9)$$

where C is the threefold rotation operator. Therefore, $\sigma^{[111]} \neq 0$, and finite anomalous Hall conductivity can occur in the plane parallel to the DW.

D. Unconventional AHE at the antiferromagnetic domain walls of $Nd_2Ir_2O_7$ thin films

When H is applied parallel to the [111] direction, DWs are expected to form within the (111) plane. Among the possible

DW orientations (see Appendix A), in a zero H field, the AIAO magnetic ground state favors the formation of DWs within the (111) plane due to its lower frustration compared with other possible orientations [41,42]. Moreover, a magnetization experiment on a $Cd_2Os_2O_7$ single crystal, another AIAO ordered pyrochlore structure, showed that the plane of DW formation prefers to orient normal to the direction of the applied H [42]. Thus, in our experimental geometry, DWs with the (111) plane orientation should play a significant role in magnetotransport results.

Figure 6(b) shows the H-dependent ρ_{xy} at 2 K, from which we subtract the ordinary term that varies linearly with H. As mentioned earlier, we should interpret this unconventional Hall resistivity as a combination of the bulk AHE and the DW AHE. The bulk AHE is shown as the blue curve, estimated by following the procedure in Sec. IV B. To obtain the Hall resistivity attributable to DW AHE, we have subtracted the bulk AHE from the experimental values. The red circles in Fig. 6(b) show the remaining contribution.

Note that the maximum value of the remaining Hall resistivity $\Delta\rho_{xy} \sim 15\,\mu\Omega\,\mathrm{cm}$ is twice as large as the saturated Hall resistivity value of $\sim 8\,\mu\Omega\,\mathrm{cm}$. The obtained maximum value of the red circles ($\sim$2 T) is also in reasonable agreement with $\mu_0 H_C^{\mathrm{Ir}}$ ($\sim$3 T) from MR where a DW conductance contribution played a significant role. The red circles follow the Gaussian functions used to fit $\mathrm{MR}_{\mathrm{Asym,\ FIT}}(H)$ [see Eq. (2)]. This implies that broad DW switching occurrs upon an applied H, which is consistent with our MR analysis. Moreover, the quadratic dependence of the DW anomalous Hall resistivity on longitudinal resistivity indicates that intrinsic AHEs arose at $\mu_0 H_C^{\mathrm{Ir}}$ ($\sim$3 T) (see Appendix B). Thus, our results indicate that the humplike ρ_{xy} signal originates from the DW AHE.

Figure 6(c) shows a contour plot of the ρ_{xy}, from which we subtract the ordinary term, as a function of both T and H. The contour plot also supports a large enhancement of AHE due to DWs. For a given T, the H value at which ρ_{xy} reaches its maximum is correlated with the value of H_c^{Ir} from MR. This implies that the large density of DWs near H_c^{Ir} can result in a maximized contribution to the AHE. The peak value of the humplike Hall resistivity is also highly enhanced below $T_{\mathrm{N}}^{\mathrm{Nd}}$, which supports the idea of a strong coupling between Ir and Nd sublattices via the f-d exchange interaction.

It has already been observed experimentally that the DWs of $Nd_2Ir_2O_7$ have a much higher conductivity than bulk $Nd_2Ir_2O_7$. Their conductivity is approximately one order of magnitude larger [15,43]. Hence, the DW AHE may be significantly enhanced in $Nd_2Ir_2O_7$ thin films. In comparison, Hall data on $Sm_2Ir_2O_7$ thin films, in which the DW conductance is lower than that of the bulk [44], do not reveal any hysteretic AHE, as shown in Fig. 10 in Appendix C. This observation also indirectly supports that the hysteretic humplike AHE observed in $Nd_2Ir_2O_7$ thin films originates from DW conduction.

V. SUMMARY

In summary, we observe a large AHE in an AFM $Nd_2Ir_2O_7$ thin film, which is induced mainly by the DWs. The strong f-d exchange interaction effectively lowers the energy barrier for Ir domain switching, such that a small magnetic field can be used to control the Ir-DW. Eventually, effective Ir-domain switching induces an intrinsic AHE from the Berry curvature at the DW leading to a large DW AHE, $\sim 15\,\mu\Omega\,\mathrm{cm}$ at 2 K. Given the observation of AHE at DWs, we suggest that $Nd_2Ir_2O_7$ is a fertile area for the discovery and investigation of new topological phenomena. As the DW-conducting channels of $Nd_2Ir_2O_7$ are attributable to the fact that the system lies close to the topological Weyl semimetal phase, the observed DW-driven AHE provides additional evidence that the system exhibits important topological properties.

ACKNOWLEDGMENTS

We are grateful to E. S. Choi for helpful discussions and assistance with high magnetic field measurements. We wish to thank Y. Kozuka and K. Ueda for helpful discussions. This work was supported by the Research Center Program of the Institute for Basic Science in Korea (Grants No. IBS-R009-D1 and No. IBS-R009-G1). The work at the National High Magnetic Field Laboratory was supported by the National Science Foundation Cooperative Agreement Grant No. DMR-1157490 and the State of Florida. T.O. and B.J.Y. acknowledge the support of the Research Resettlement Fund for new faculty of Seoul National University and the Basic Science Research Program through the National Research Foundation of Korea funded by the Ministry of Education (Grant No. 0426-20150011). J.H.G. and A.S. acknowledge the support of National Science Foundation Grant No. DMR-1454200.

APPENDIX A: ORIENTATION OF THE MAGNETIC DOMAIN-WALL PLANE

The local structures of DWs are considered in terms of the classical spin model. The stability of DWs has been studied in the extreme limit of the strong Ising anisotropy [42]. Three types of spin configurations are possible at local structures of DWs: Ir-AIAO or Ir-AOAI, Ir-3I1O or Ir-1I3O, and Ir-2I2O. The energies of these configurations are given as $E_{\mathrm{AIAO}} = -6\,J_{\mathrm{eff}}$, $E_{3\mathrm{I}3\mathrm{O}} = 0$, and $E_{2\mathrm{I}2\mathrm{O}} = 2\,J_{\mathrm{eff}}$, where J_{eff} is the nearest-neighbor effective antiferromagnetic interaction ($J_{\mathrm{eff}} > 0$). The stability between these DWs can be compared in terms of these energies. The energy of a DW is defined

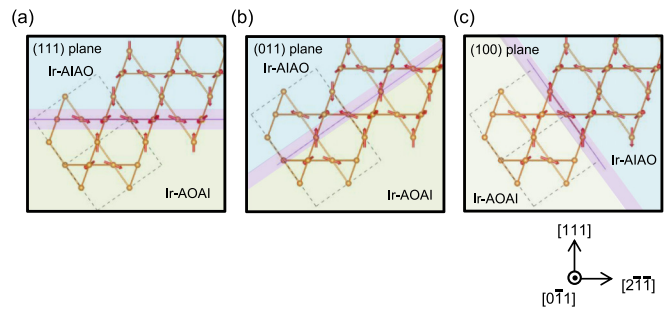

FIG. 8. Schematic diagrams of various local structures of DWs. Blue and light green regions indicate the AIAO and AOAI Ir spin ordered domain, respectively. The purple region indicates the DW between two distinct domains. The dashed line indicates the unit cell of $Nd_2Ir_2O_7$. (a) Spin structures of the (111) DW consisting of 1I3O tetrahedra and (b) the (011) DW consisting of 1I3O tetrahedra. (c) Spin structures of the (100) DW consisting of 2I2O tetrahedra.

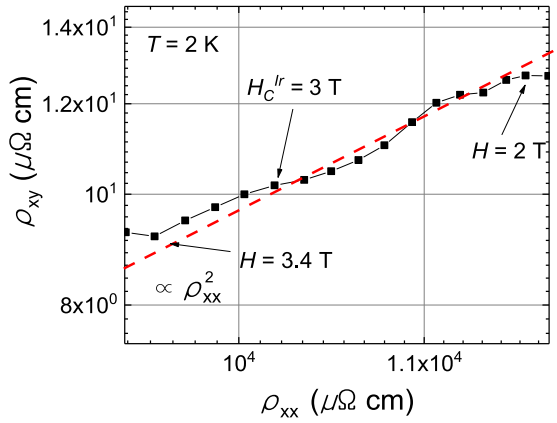

FIG. 9. The ρ_{xx} vs ρ_{xy} plot at 2 K under the H field along the [111] direction, which is close to coercive field H_c^{Ir}. The dashed lines are to guide the eyes. Note that both the x axis and y axis are depicted in the log scale.

as the energy cost per area (A) and is calculated as $E_{\mathrm{DW}} = 2(E_{2\mathrm{I2O}} - E_{\mathrm{AIAO}})/A = 16\,J_{\mathrm{eff}}/A$ for a (100) DW consisting of Ir-2I2O tetrahedra [see Fig. 8(c)]. Similarly, the {111} and {011} DWs containing only Ir-1I3O tetrahedra as depicted in Figs. 8(a) and 8(b) are most stable with $E_{\mathrm{DW}} \sim 13.9\,J_{\mathrm{eff}}/A$, and $\sim$17.0 J_{eff}/A, respectively.

Among these possible DWs configurations, the {111} DW is the most preferable state due to its lowest E_{DW} value. Other types of DWs also can be formed, and can be understood as the combination of the above DW configurations. Particularly, within H along [111], the energy cost of (111) plane DW formation should be lower. Therefore, in our experimental geometry, the $Nd_2Ir_2O_7$ thin film should contain the (111) plane DW with H along the [111] direction.

APPENDIX B: QUADRATIC DEPENDENCE OF THE DOMAIN-WALL ANOMALOUS HALL RESISTIVITY ON LONGITUDINAL RESISTIVITY

The quadratic dependence of the DW anomalous Hall resistivity on the longitudinal resistivity indicates that the intrinsic AHE arises at $H \sim H_c^{\mathrm{Ir}}$, where a large DW contribution plays a role. Based on the intrinsic mechanism, ρ_{xy} is known to exhibit a power-law dependence on ρ_{xx}, i.e., $\rho_{xy} \sim \rho_{xx}^a$, with an exponent $a\sim$2.0 [45]. Near the domain switching region, where the DW contribution is largest, the power-law dependence of ρ_{xy} shows $\rho_{xy} \sim \rho_{xx}^2$ (see Fig. 9). Ferromagnetic ordering at the DW may induce the intrinsic AHE, which is usually observed in ferromagnets.

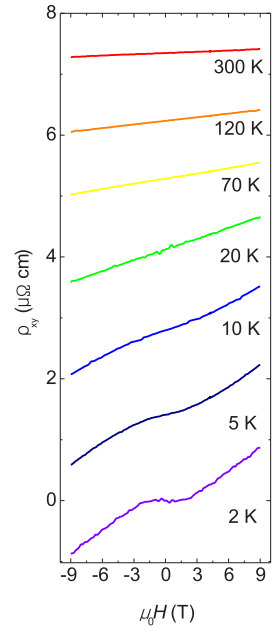

FIG. 10. H dependence of Hall resistivity of $\sim$170-nm-thick $Sm_2Ir_2O_7$ thin film taken with $H \parallel$ [111] at various temperatures.

APPENDIX C: HALL MEASUREMENT ON OTHER RARE-EARTH PYROCHLORE IRIDATE THIN FILMS

We measure the Hall resistivity of a $Sm_2Ir_2O_7$/YSZ (111) thin film, which has a thickness of $\sim$170 nm. The current path is taken along the $[1\bar{1}0]$ direction, and H is always oriented perpendicular to the current direction, which is along the [111] direction. Figure 10 shows the ρ_{xy} curves at various T, including the value at $T_{\mathrm{N}}^{\mathrm{Ir}} \sim 120$ K of $Sm_2Ir_2O_7$. At high temperatures (above $\sim$70 K), the Hall resistivity has a linear dependence on H, which is typical behavior for the ordinary Hall effect. However, at lower temperatures (below $\sim$20 K), we observe an anomaly that presumably arises due to the Ir moment canting effect. In comparison to the Hall results for the $Nd_2Ir_2O_7$ thin film, no hysteresis occurs. We speculate that this different Hall behavior is induced by the different DW conductance.

[1] J. Seidel, L. W. Martin, Q. He, Q. Zhan, Y.-H. Chu, A. Rother, M. E. Hawkridge, P. Maksymovych, P. Yu, M. Gajek, N. Balke, S. V. Kalinin, S. Gemming, F. Wang, G. Catalan, J. F. Scott, N. A. Spaldin, J. Orenstein, and R. Ramesh, Nat. Mater. **8**, 229 (2009).

[2] D. Meier, J. Seidel, A. Cano, K. Delaney, Y. Kumagai, M. Mostovoy, N. A. Spaldin, R. Ramesh, and M. Fiebig, Nat. Mater. **11**, 284 (2012).

[3] W. Wu, Y. Horibe, N. Lee, S.-W. Cheong, and J. R. Guest, Phys. Rev. Lett. **108**, 077203 (2012).

[4] G. Catalan, J. Seidel, R. Ramesh, and J. F. Scott, Rev. Mod. Phys. **84**, 119 (2012).

[5] J. Matsuno, N. Ogawa, K. Yasuda, F. Kagawa, W. Koshibae, N. Nagaosa, Y. Tokura, and M. Kawasaki, Sci. Adv. **2**, e1600304 (2016).

[6] X. Z. Yu, Y. Onose, N. Kanazawa, J. H. Park, J. H. Han, Y. Matsui, and Y. Nagaosa, Nature (London) **465**, 901 (2011).

[7] E. G. Tveten, T. Müller, J. Linder, and A. Brataas, Phys. Rev. B **93**, 104408 (2016).

[8] X. Wan, A. M. Turner, A. Vishwanath, and S. Y. Savrasov, Phys. Rev. B **83**, 205101 (2011).

[9] W. W.-Krempa, G. Chen, Y. B. Kim, and L. Balents, Ann. Rev. Condens. Mat. Phys. **5**, 57 (2014).

[10] K. Matsuhira, M. Wakeshima, R. Nakanishi, T. Yamada, A. Nakamura, W. Kawando, S. Takagi, and Y. Hinatsu, J. Phys. Soc. Jpn. **76**, 043706 (2007).

[11] K. Matsuhira, M. Wakeshima, Y. Hinatsu, and S. Takagi, J. Phys. Soc. Jpn. **80**, 094701 (2011).

[12] E. Y. Ma, Y.-T. Cui, K. Ueda, S. Tang, K. Chen, N. Tamura, P. M. Wu, J. Fujioka, Y. Tokura, and Z.-X. Shen, Science **350**, 538 (2015).

[13] G. Chen and M. Hermele, Phys. Rev. B **86**, 235129 (2012).

[14] Y.-P. Huang, G. Chen, and M. Hermele, Phys. Rev. Lett. **112**, 167203 (2014).

[15] K. Ueda, J. Fujioka, B.-J. Yang, J. Shiogai, A. Tsukazaki, S. Nakamura, S. Awaji, N. Nagaosa, and Y. Tokura, Phys. Rev. Lett. **115**, 056402 (2015).

[16] K. Ueda, J. Fujioka, Y. Takahashi, T. Suzuki, S. Ishiwata, Y. Taguchi, and Y. Tokura, Phys. Rev. Lett. **109**, 136402 (2012).

[17] B.-J. Yang and N. Nagaosa, Phys. Rev. Lett. **112**, 246402 (2014).

[18] M.-T. Suzuki, T. Koretsune, M. Ochi, and R. Arita, Phys. Rev. B **95**, 094406 (2017).

[19] M. E. Fisher and A. E. Ferdinand, Phys. Rev. Lett. **19**, 169 (1967).

[20] E. H. P. Cordfunke and G. Meyer, Recl. des Trav. Chim. des Pays-Bas **81**, 495 (1962).

[21] J. C. Gallagher, B. D. Esser, R. Morrow, S. R. Dunsiger, R. E. A. Williams, P. M. Woodward, D. W. McComb, and F. Y. Yang, Sci. Rep. **6**, 22282 (2016).

[22] W. C. Yang, Y. T. Xie, W. K. Zhu, K. Park, A. P. Chen, Y. Losovyj, Z. Li, H. M. Liu, M. Starr, J. A. Acosta, C. G. Tao, N. Li, Q. X. Jia, J. J. Heremans, and S. X. Zhang, Sci. Rep. **7**, 7740 (2017).

[23] K. T. Jacob, T. H. Okabe, T. Uda, and Y. Waseda, Electrochim. Acta **45**, 1963 (2000).

[24] T. C. Fujita, Y. Kozuka, M. Uchida, A. Tsukazaki, T. Arima, and M. Kawasaki, Sci. Rep. **5**, 9711 (2015).

[25] M. Nakayama, T. Kondo, Z. Tian, J. J. Ishikawa, M. Halim, C. Bareille, W. Malaeb, K. Kuroda, T. Tomita, S. Ideta, K. Tanaka, M. Matsunami, S. Kimura, N. Inami, K. Ono, H. Kumigashira, L. Balents, S. Nakatsuji, and S. Shin, Phys. Rev. Lett. **117**, 056403 (2016).

[26] K. Tomiyasu, K. Matsuhira, K. Iwasa, M. Watahiki, S. Takagi, M. Wakeshima, Y. Hinatsu, M. Yokoyama, K. Ohoyama, and K. Yamada, J. Phys. Soc. Jpn. **81**, 034709 (2012).

[27] Under the H field, both spin canting and domain switching can induce MR. However, the irreversible processes, such as hysteresis, can be explained in terms of the domain switching.

[28] V. K. Wadhawan, *Introduction to Ferroic Materials* (CRC, Boca Raton, FL, 2000).

[29] K. G.Webbera, H. C. Robinson, G. A. Rossetti, and C. S. Lynch, Acta Mater. **56**, 2744 (2008).

[30] Z. Zhao, K. Bowman, and R. E. García, J. Am. Ceram. Soc. **95**, 1619 (2012).

[31] X. G. Wen, F. Wilczek, and A. Zee, Phys. Rev. B **39**, 11413 (1989).

[32] K. Ohgushi, S. Murakami, and N. Nagaosa, Phys. Rev. B **62**, R6065 (2000).

[33] Y. Taguchi, Y. Oohara, H. Yoshizawa, N. Nagaosa, and Y. Tokura, Science **291**, 2573 (2001).

[34] Y. Taguchi, T. Sasaki, S. Awaji, Y. Iwasa, T. Tayama, T. Sakakibara, S. Iguchi, T. Ito, and Y. Tokura, Phys. Rev. Lett. **90**, 257202 (2003).

[35] P. Bruno, V. K. Dugaev, and M. Taillefumier, Phys. Rev. Lett. **93**, 096806 (2004).

[36] Y. Machida, S. Nakatsuji, Y. Maeno, T. Tayama, T. Sakakibara, and S. Onoda, Phys. Rev. Lett. **98**, 057203 (2007).

[37] N. Nagaosa, J. Sinova, S. Onoda, A. H. MacDonald, and N. P. Ong, Rev. Mod. Phys. **82**, 1539 (2010).

[38] C. Sürgers, G. Fischer, P. Winkel, and H. v. Löhneysen, Nature Commun. **5**, 3400 (2014).

[39] S. Nakatsuji, N. Kiyohara, and T. Higo, Nature (London) **527**, 212 (2015).

[40] T. Arima, J. Phys. Soc. Jpn. **82**, 013705 (2013).

[41] S. Tardif, S. Takeshita, H. Ohsumi, J. I. Yamaura, D. Okuyama, Z. Hiroi, M. Takata, and T. H. Arima, Phys. Rev. Lett. **114**, 147205 (2015).

[42] H. T. Hirose, J. Yamaura, and Z. Hiroi, Sci. Rep. **7**, 42440 (2017).

[43] Z. Tian, Y. Kohama, T. Tomita, H. Ishizuka, T. H. Hsieh, J. J. Ishikawa, K. Kindo, L. Balents, and S. Nakatsuji, Nat. Phys. **12**, 134 (2016).

[44] K. Ueda, J. Fujioka, C. Terakura, and Y. Tokura, Phys. Rev. B **92**, 121110(R) (2015).

[45] S. Onoda, N. Sugimoto, and N. Nagaosa, Phys. Rev. Lett. **97**, 126602 (2006).